Shining in the dark: the spectral evolution of the first black holes

Fabio Pacucci, Andrea Ferrara, Marta Volonteri, Guillaume Dubus

Shining in the dark: the spectral evolution of the first black holes

Fabio Pacucci,[1]★ Andrea Ferrara,[1,2] Marta Volonteri[3] and Guillaume Dubus[3,4]

[1]*Scuola Normale Superiore, Piazza dei Cavalieri, I-7 56126 Pisa, Italy*
[2]*Kavli Institute for the Physics and Mathematics of the Universe (WPI), Todai Institutes for Advanced Study, The University of Tokyo, 5-1-5 Kashiwanoha, Kashiwa 277-8583, Japan*
[3]*Sorbonne Universités, UPMC Univ Paris 06, CNRS, UMR 7095, Institut d'Astrophysique de Paris, F-75014 Paris, France*
[4]*Université Grenoble Alpes, CNRS, UMR 5274, IPAG, F-38000 Grenoble, France*

ABSTRACT

Massive black hole (MBH) seeds at redshift $z \gtrsim 10$ are now thought to be key ingredients to explain the presence of the supermassive ($10^{9-10}\,\mathrm{M_\odot}$) black holes in place <1 Gyr after the big bang. Once formed, massive seeds grow and emit copious amounts of radiation by accreting the left-over halo gas; their spectrum can then provide crucial information on their evolution. By combining radiation-hydrodynamic and spectral synthesis codes, we simulate the time-evolving spectrum emerging from the host halo of a MBH seed with initial mass $10^5\,\mathrm{M_\odot}$, assuming both standard Eddington-limited accretion, or slim accretion discs, appropriate for super-Eddington flows. The emission occurs predominantly in the *observed* infrared-submm (1-1000 μm) and X-ray (0.1–100 keV) bands. Such signal should be easily detectable by *JWST* around ~ 1 μm up to $z \sim 25$, and by *ATHENA* (between 0.1 and 10 keV, up to $z \sim 15$). Ultra-deep X-ray surveys like the *Chandra* Deep Field South could have already detected these systems up to $z \sim 15$. Based on this, we provide an upper limit for the $z \gtrsim 6$ MBH mass density of $\rho_\bullet \lesssim 2.5 \times 10^2\,\mathrm{M_\odot\,Mpc^{-3}}$ assuming standard Eddington-limited accretion. If accretion occurs in the slim disc mode the limits are much weaker, $\rho_\bullet \lesssim 7.6 \times 10^3\,\mathrm{M_\odot\,Mpc^{-3}}$ in the most constraining case.

Key words: accretion, accretion discs – black hole physics – radiative transfer – quasars: supermassive black holes – dark ages, reionization, first stars – early Universe.

1 INTRODUCTION

The cosmic epoch in the redshift range $10 \lesssim z \lesssim 30$ was characterized by the formation of the first stars (Pop III) and of the first black holes (see Volonteri 2010; Bromm & Yoshida 2011; Volonteri & Bellovary 2012; Haiman 2013 for recent reviews). Detecting these sources directly is at, or beyond, the sensitivity edge of current observatories. While recently Sobral et al. (2015) have shown that a very luminous Lyα emitter at $z \approx 6.6$ may be consistent with having a mixed composition of Pop III and second-generation (Pop II) stars, to date there are no confirmed observations of the first black holes, partly due to the uncertainty on their observational signatures. The next generation of observatories will most likely detect the first glimpses of light in the Universe, both in the electromagnetic spectrum (e.g. ALMA, *JWST*, *ATHENA*) and in the gravitational waves domain (e.g. e-LISA, DECIGO).

The formation process of the first black holes is likely to produce a strong imprint on their observational signatures, as well as on their mass growth. The standard theory of Eddington-limited accretion predicts that black holes grow in mass over a time-scale $\sim 0.045\epsilon_{0.1}$ Gyr, where $\epsilon_{0.1}$ is the matter–energy conversion factor normalized to the standard value of 10 per cent. With black hole seeds of initial mass $\sim 100\,\mathrm{M_\odot}$, formed at the end of the very short (~ 1–10 Myr) lifetime of Pop III stars, it is, at best, challenging to explain recent observations of optically bright quasars with $M_\bullet \sim 10^{9-10}\,\mathrm{M_\odot}$ at $z \sim 7$ (Mortlock et al. 2011; Wu et al. 2015). An alternative, attractive solution is based on massive black hole (MBH) seeds ($10^{3-5}\,\mathrm{M_\odot}$) appearing at $z \sim 10$–15, giving a jump start to the growth process (e.g. Begelman, Volonteri & Rees 2006; Lodato & Natarajan 2006; Spaans & Silk 2006). Under specific conditions (Bromm & Loeb 2003; Begelman et al. 2006; Volonteri, Lodato & Natarajan 2008; Shang, Bryan & Haiman 2010; Johnson et al. 2012; Agarwal et al. 2014), the collapse of a primordial atomic-cooling halo may lead to the formation of MBHs with a birth mass function peaked at $M_\bullet \sim 2 \times 10^5\,\mathrm{M_\odot}$ (Ferrara et al. 2014). The subsequent gas accretion from the host halo leads to further growth into $\gtrsim 10^7\,\mathrm{M_\odot}$ objects.

The expected abundance of MBHs is largely unconstrained. Salvaterra et al. (2012) and Treister et al. (2013) provided upper limits of order $\rho_\bullet \lesssim 10^{3-4}\,\mathrm{M_\odot\,Mpc^{-3}}$, using the X-ray background and the stacked X-ray luminosity of high-redshift galaxies, respectively.

★ E-mail: fabio.pacucci@sns.it

Upper limits for the $z = 6$ MBH mass density provided by Willott (2011), Fiore et al. (2012) and Cowie, Barger & Hasinger (2012) are even lower ($\rho_\bullet \lesssim 10^{2-3} \, \mathrm{M_\odot \, Mpc^{-3}}$), although none of these constraints takes into account Compton-thick sources that can be buried deep inside dense nuclei in proto-galaxies. Yue et al. (2013, 2014) noted that if MBHs are responsible for the near-infrared background fluctuations, their high-redshift mass density should be comparable to the present-day value: $\rho_\bullet(z = 0) \sim 2 \times 10^5 \, \mathrm{M_\odot \, Mpc^{-3}}$, see Yu & Tremaine (2002). The population of high-redshift MBHs would produce gravitational waves, during their collapse (Pacucci, Ferrara & Marassi 2015) or ensuing MBH–MBH mergers (Sesana, Volonteri & Haardt 2007; Sesana et al. 2011), detectable with upcoming observatories.

Our previous works (Pacucci & Ferrara 2015; Pacucci, Volonteri & Ferrara 2015) focused, through accurate one-dimensional (1D) radiation-hydrodynamic simulations, on the dynamical evolution of $z \sim 10$ MBH seeds with initial mass $M_\bullet \sim 10^{3-6} \, \mathrm{M_\odot}$, embedded in dark matter haloes with total mass $M_h \sim 10^8 \, \mathrm{M_\odot}$ and accreting in the standard Eddington-limited scenario, or including a model for super-Eddington accretion through slim discs (see also Volonteri & Rees 2005; Volonteri, Silk & Dubus 2015). In the present work we focus on their emission spectrum with three objectives: (i) predict the time evolution of the spectrum, (ii) assess the observability with current (*Chandra* Deep Field South, CDF-S) and future (*JWST*, *ATHENA*) surveys, and (iii) estimate the mass density $\rho_\bullet$ of high-redshift MBHs.

The outline of this paper is as follows. In Section 2 we describe the physical and numerical implementation, while in Section 3 we present our results for the spectral evolution of high-redshift MBHs. Finally, in Section 4 we provide some further discussion and the conclusions. We adopt recent Planck (Planck Collaboration XIII et al. 2015) cosmological parameters throughout: $(\Omega_m, \Omega_\Lambda, \Omega_b, h, n_s, \sigma_8) = (0.32, 0.68, 0.05, 0.67, 0.96, 0.83)$.

2 PHYSICAL AND NUMERICAL IMPLEMENTATION

The present work is based on radiation-hydrodynamic simulations post-processed with CLOUDY, a spectral synthesis code (Ferland et al. 2013).

The physical framework is the following: a high-redshift ($z = 10$) MBH seed with initial mass $10^5 \, \mathrm{M_\odot}$ is located at the centre of a dark matter halo with primordial composition and total mass $M_h \sim 10^8 \, \mathrm{M_\odot}$ ($T_{vir} \sim 10^4 \, \mathrm{K}$). The MBH accretes mass from the inner parts (within $\sim 10 \, \mathrm{pc}$) of the host halo until complete gas depletion.

Our radiation-hydrodynamic code takes into account the frequency-integrated radiative transfer through the gas, with appropriate: (i) cooling and heating terms, (ii) matter-to-radiation coupling, and (iii) energy propagation through a two-stream approximation method. The code computes the accretion rate through the inner boundary of the simulation domain, from which we derive the total bolometric energy radiated by accretion, assuming a radiatively efficient or inefficient disc. The full *frequency-dependent* radiative transfer through the host halo is then performed in a post-processing step using CLOUDY. This code computes the detailed time-evolving spectrum emerging from the host halo using as input the matter distribution obtained from our radiation-hydrodynamics simulations and the realistic irradiation spectrum at the inner boundary, scaled to the appropriate bolometric luminosity. Additional details are given in Sections 2.1 and 2.2.

2.1 Dynamics and thermodynamics

Our radiation-hydrodynamic code (see Pacucci & Ferrara 2015 for an extensive description) solves the 1D spherically symmetric equations of hydrodynamics and a frequency-integrated version of radiative transfer equations. The code evolves self-consistently the radial component of the standard system of ideal, non-relativistic Euler's equations (neglecting viscosity, thermal conduction and magnetic fields) for a gas accreting, with no angular momentum, on to the central MBH, assumed at rest and already formed at the time $t = 0$, with a given initial mass $M_\bullet(t = 0)$. The simulation domain spans from 0.1 to 10 pc, largely encompassing the characteristic spatial scale for accretion, the Bondi radius:

$$R_B = \frac{GM_\bullet}{c_{s(\infty)}^2} \sim 3.0 \, \mathrm{pc} \,, \qquad (1)$$

where G is the gravitational constant and $c_{s(\infty)} = \sqrt{\gamma R T_\infty / \mu} \sim 12 \, \mathrm{km \, s^{-1}}$ is the sound speed at large distances from the accretion boundary; $\gamma = 5/3$ is the ratio of specific heats, R is the gas constant, T is the gas temperature and $\mu = 1.15$ is the mean molecular weight for a primordial H–He composition gas with helium fraction $Y_P = 0.24665$ (Planck Collaboration XIII et al. 2015) and no metals. For a $10^5 \, \mathrm{M_\odot}$ object, the inner boundary of our spatial domain is $\sim 10^7$ times larger than the Schwarzschild radius and $\sim 10^5$ times larger than the centrifugal radius, i.e. the spatial scale below which deviations from spherical symmetry become important and an accretion disc may form. Moreover, the angular momentum transfer in the outwards direction of the accretion flow is very efficient, due to gravitational torques induced by dark matter and gas distributions of the halo (Choi, Shlosman & Begelman 2015). The gas loses its angular momentum efficiently and flows well beyond its centrifugal barrier. Therefore, despite its simplifications, our 1D approach is significantly helpful in acquiring physical insights on the mechanisms regulating the black hole growth. For the same reason, neglecting viscosity, thermal conduction and magnetic fields is a safe choice, since they play an important role only on spatial scales comparable with the radius of the accretion disc.

The gas accretion through the inner boundary of our spatial domain produces an accretion rate $\dot{M}_\bullet$, which in turn generates an emitted luminosity L via two different accretion models: (i) a standard Eddington-limited model in which $L = \epsilon c^2 \dot{M}$, $\epsilon = 0.1$, and (ii) a radiatively inefficient model, the slim disc, in which $L \propto \ln(\dot{M}_\bullet)$ and $\epsilon \lesssim 0.04$ is a function of $\dot{M}_\bullet$. The main physical quantity which determines the properties of the accretion disc, and consequently the radiative efficiency, is the accretion rate. Accretion of gas at moderate rates ($0.01 \lesssim f_{Edd} \lesssim 1$) is expected to form a radiatively efficient, geometrically thin and optically thick accretion disc, which is typically modelled with the standard α-disc model (Shakura & Sunyaev 1973). In the Shakura and Sunyaev disk the radiative efficiency is determined only by the location of the innermost stable circular orbit, which in turn depends only on the spin of the black hole, and it varies between ~ 6 and ~ 32 per cent for a non-spinning and a maximally spinning black hole, respectively (Thorne 1974). In a supercritical ($f_{Edd} > 1$) accretion environment the structure of the accretion disc is, instead, expected to be geometrically and optically thick and radiatively inefficient (but see Jiang, Stone & Davis 2014; McKinney, Dai & Avara 2015). The most common solution proposed for such accretion flows is the slim disc (Paczynski & Abramowicz 1982; Abramowicz et al. 1988; Mineshige et al. 2000; Sadowski 2009, 2011; McKinney et al. 2014). In these scenarios, part of the energy produced inside the disc is advected inwards (see, e.g. Abramowicz & Fragile 2013;

Lasota 2015) out to a spatial scale named the photon trapping radius ($R_{tr} \sim R_s f_{Edd}$, where R_s is the Schwarzschild radius). Therefore, only a fraction of the photons produced in the accretion disk is able to free stream out of R_{tr}: consequently, the effective radiation and radiation pressure escaping to infinity is decreased (see, e.g. Begelman 1978; Ohsuga et al. 2002). While the slim disc solution is the simplest and most tested model for supercritical accretion, alternatives exist, e.g the ZEro-BeRnoulli Accretion (ZEBRA; Coughlin & Begelman 2014) and the ADiabatic Inflow-Outflow Solutions (ADIOS; Blandford & Begelman 1999; Begelman 2012) models. These theoretical models also include a parameter which describes the fraction of the inflowing mass which is lost due to radiation pressure.

Radiation pressure accelerates the gas via

$$a_{rad}(r) = \frac{\kappa(\rho, T)L(r)}{4\pi r^2 c} , \quad (2)$$

where the gas opacity $\kappa(\rho, T)$ includes Thomson and bound-free terms, with the inclusion of a temperature dependence (Begelman, Rossi & Armitage 2008). The radiation pressure may be able to temporarily interrupt the gas inflow, resulting in an intermittent accretion and outflows. The physical parameters regulating this occurrence are investigated in Pacucci et al. (2015).

We assume that the gas initially follows the isothermal ($T \sim 10^4$ K) density profile derived from the simulations in Latif et al. (2013a), approximated by the functional form:

$$\rho(r) = \frac{\rho_0}{1 + (r/a)^2} , \quad (3)$$

where a is the core radius and ρ_0 is the central density. To understand how the matter distribution influences both the accretion and the emerging spectrum (through the hydrogen column density), we implemented two different density profiles, both of them yielding a gas mass $\sim 10^7 \, M_\odot$: (i) a high-density profile (HDP) with a central density $\rho_0 = 10^{-12}$ g cm^{-3} and a core radius $a = 0.002$ pc, and (ii) a low-density profile (LDP) with a central density $\rho_0 = 10^{-18}$ g cm^{-3} and a core radius $a = 2$ pc. The LDP may be thought as the density profile resulting after the formation of a MBH of mass $\sim 10^5 \, M_\odot$ at the halo centre (see Latif et al. 2013b; Latif, Niemeyer & Schleicher 2014), while in the HDP case the seed formed is very small ($\lesssim 10^3 \, M_\odot$). A density floor of 10^{-24} g cm$^{-3} \sim 1$ cm^{-3}, a factor at least 10^6 times smaller than the central density for both profiles, is imposed for numerical stability reasons. In summary, we have four models: standard accretion – LDP, standard accretion – HDP, slim disc accretion – LDP, slim disk accretion – HDP.

2.2 Spectrum

Our code evolves the system in time until gas depletion and provides CLOUDY with data to compute the spectrum emerging from the host halo. This code takes into account: (i) the spatial profiles for hydrogen number density $n_H(r)$ and temperature $T(r)$, (ii) the source spectrum of the central object, and (iii) the bolometric luminosity L of the source, computed self-consistently from $\dot{M}_\bullet$. The spherical cloud of gas is assumed to be metal free, so that only H and He recombination lines are present. The addition of a small amount of metals, formed by the first Pop III stars, would increase the number of lines and the absorption of high-energy photons. The source spectral energy distribution is taken from Yue et al. (2013) and can be described as the sum of three components: (i) a multicolour blackbody, (ii) a power law, and (iii) a reflection component. The source spectrum is extended from far-infrared to hard X-ray (~ 1 MeV).
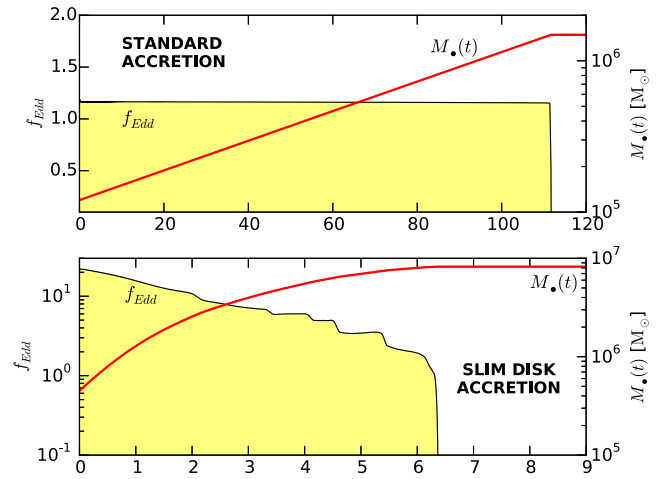

Figure 1. Time evolution of the Eddington factor f_{Edd} and of the black hole mass $M_\bullet$, in the standard accretion – LDP (top) and the slim disc accretion – LDP (bottom) scenarios. The Eddington ratio is reported as a running average over periods of ~ 0.1 Myr.

3 RESULTS

We describe in the following the standard accretion – LDP case, and discuss the differences with the other cases when needed.

The balance between the inwards gravitational acceleration and the outwards radiation pressure keeps the accretion rate close to the Eddington level ($f_{Edd} \approx 1.2$) for most of the time, ensuring a continuous accretion. The top panel of Fig. 1 shows the time evolution of f_{Edd} and of $M_\bullet$ in this accretion scenario. Defining the duty cycle, $\mathcal{D}$, as the fraction of time spent accreting during the total evolutionary time of the system, we find that in the LDP cases $\mathcal{D} = 1$, while other accretion scenarios may be characterized by quiescent phases ($\mathcal{D} < 1$, see Table 1). The system evolves for ~ 120 Myr, until complete depletion of the $\sim 10^7 \, M_\odot$ gas reservoir within ~ 10 pc. However, this time-scale is a lower limit, since in a real galaxy the gas would extend much further.

Fig. 2 (top panel) shows the time evolution of the bolometric luminosity emitted at the inner boundary, before traversing the host halo gas. The corresponding Eddington luminosity
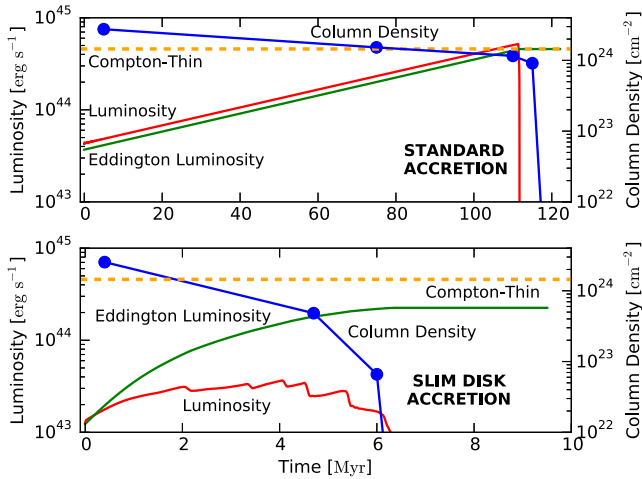
$$L_{Edd} \equiv \frac{4\pi G M_\bullet c}{\kappa_T} \propto M_\bullet , \quad (4)$$

with κ_T being the Thomson opacity, is also shown for comparison. The luminosity increases for the first ~ 115 Myr, reaching a peak of $\sim 5 \times 10^{44}$ erg s^{-1} and is, on average, mildly super-Eddington as long as the amount of gas is sufficient to sustain this accretion rate. Afterwards, the luminosity plummets, when all the available gas has been consumed. For comparison, the interested reader is referred to Pacucci & Ferrara (2015), where a plot of the same physical quantities is shown in fig. 8. Moreover, Fig. 2 also shows the values of the hydrogen column density, N_H, computed at selected times ($t_s = 5, 75, 110, 115, 120$ Myr) when also the emergent spectrum is computed. The system is initially Compton thick ($N_H \gtrsim 1.5 \times 10^{24}$ cm^{-2}, see the horizontal line). As the gas is progressively accreted by the MBH, N_H steadily decreases before a sudden drop ($t_s \approx 115$ Myr) corresponding to the remaining gas evacuation by radiation pressure. Table 1 lists duty cycles and accretion time-scales for all four models.

The bottom panels of Figs 1 and 2 show the time evolution of f_{Edd}, $M_\bullet$, L and N_H in the slim disc – LDP case. In this accretion scenario, the Eddington rate reaches high values ($f_{Edd} \sim 20$) only

Table 1. Accretion history and CDF-S observability for a MBH seed with initial mass $M_\bullet = 10^5\,M_\odot$ in the four indicated accretion scenarios.
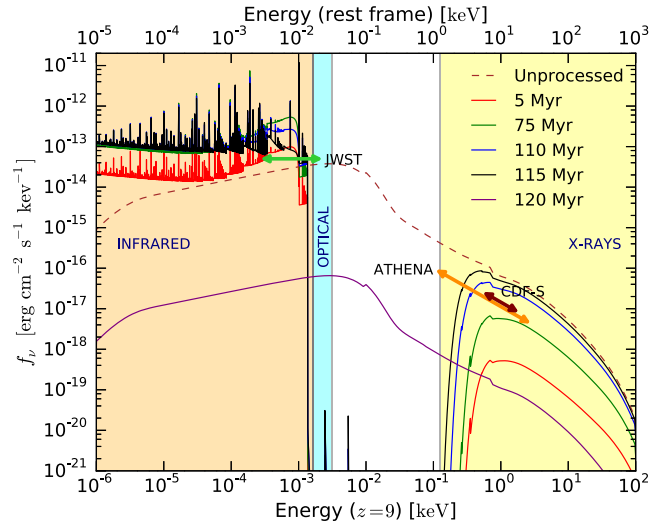
Accretion scenario	Observable	$t_{\rm end}$ (Myr)	$\mathcal{D}$	$t_{\rm det}$ (Myr)	$\mathcal{F}$	$\rho_\bullet$ ($M_\odot$ Mpc^{-3})
Standard accretion – LDP	YES	120	1.0	30	0.045	$\lesssim 2.5 \times 10^2$
Standard accretion – HDP	YES	240	0.4	110	0.16	$\lesssim 1.8 \times 10^2$
Slim disc accretion – LDP	NO	7	1.0	0	0	No constraints
Slim disc accretion – HDP	YES	12	1.0	1	0.0015	$\lesssim 7.6 \times 10^3$

Figure 2. Time evolution of the bolometric luminosity emitted at the inner boundary, before traversing the host halo gas, in the standard accretion – LDP (top) and the slim disc accretion – LDP (bottom) scenarios. The luminosity is reported as a running average over periods of ~ 0.1 Myr. The corresponding Eddington luminosity, $L_{\rm Edd} \propto M_\bullet$, and the values of the hydrogen column density (blue curves, right axis) are also shown.

Figure 3. Time evolution of the spectrum emerging from the host halo for a source located at $z = 9$, in the standard accretion – LDP case. The infrared, optical and X-ray bands are highlighted with shaded regions, while the unprocessed spectrum is reported, at peak luminosity ($t = 115$ Myr), with a dashed line. The flux limits for future (*JWST*, *ATHENA*) and current (CDF-S) surveys are also shown.

for a short amount of time (~ 2 Myr), while afterwards the accretion rates are sub-Eddington. The evolution is much more rapid (the available gas is consumed in ~ 6 Myr, a factor of ~ 16 faster than in the standard case) and the host halo becomes Compton thin ($N_{\rm H} \lesssim 1.5 \times 10^{24}$ cm^{-2}) in $\lesssim 2$ Myr. As already noted in Pacucci et al. (2015), in the slim disc accretion – LDP case, the black hole is able to accrete up to ~ 80 per cent of the gas mass within ~ 10 pc, with respect to the ~ 15 per cent in the standard accretion scenario, and the black hole grows to $\sim 8 \times 10^6\,M_\odot$ in ~ 6 Myr, while in the standard case the black hole grows to $\sim 1.5 \times 10^6\,M_\odot$ in ~ 100 Myr.

3.1 Spectral evolution

The time-evolving spectrum emerging from the host halo, in the standard accretion – LDP case, is shown in Fig. 3 at $z = 9$, i.e. ~ 100 Myr after the beginning of the simulation ($z = 10$). The spectrum is composed of: (i) the continuum emitted by the source and attenuated by the gas, and (ii) the diffuse emission of the gas. Most of the energy emerges in the *observed* infrared and X-ray bands. The latter is characterized by a bell-shaped spectrum peaked around 1 keV, while in the infrared band a large number of H–He nebular lines is present. Photons with frequency shortwards than the Lyα line are absorbed by the intervening matter at column densities $N_{\rm H} \gtrsim 10^{23}$ cm^{-2} and reprocessed at lower energies, boosting the infrared emission of the halo. X-ray emission occurs predominantly within the rest-frame energy range 4 keV $< E_\gamma <$ 10 keV. The mean free path of such photons is much larger than the Hubble radius at $z = 9$: $\lambda_{\rm X} \gtrsim 8$ Gpc $\gg R_{\rm H}(z = 9) = 165$ Mpc. Hence growing MBH

seeds negligibly contribute to reionization. The increase with time of the continuum normalization in the X-ray is mainly due to the progressive rise of the bolometric luminosity of the central object. The ratio between the infrared and the X-ray continua depends on the column density, since in the Compton-thick case ($N_{\rm H} \gtrsim 1.5 \times 10^{24}$ cm^{-2}) the high-energy frequencies are heavily absorbed and reprocessed at lower energies, leading to an overall increase of the infrared emission. When the gas becomes Compton thin at ~ 75 Myr, the X-ray continuum progressively increases, while the infrared one starts to decrease. Approaching the complete gas depletion within ~ 10 pc, at ~ 120 Myr, the column density is so low (see Fig. 2, top panel) that the outgoing radiation is nearly unimpeded (the emerging spectrum is very similar to the source spectrum, reported, at peak luminosity, $t = 115$ Myr, as a dashed line) and the continuum normalization drops by ~ 3 (~ 4) orders of magnitude in the X-ray (infrared) band.

3.2 High-redshift MBH mass density

The approximate flux thresholds for two future-generation observatories (*JWST*[1] in the infrared band, *ATHENA*[2] in the X-ray) and for the CDF-S[3] survey are shown in Fig. 3. We predict that the *JWST*

---

[1] For a NIRcam observation with a signal-to-noise ratio of 10 and a total integration time of 10^4 s.
[2] For a 3σ detection with a total integration time of 3×10^5 s.
[3] Ultra-deep survey in the X-ray with a total integration time of 4×10^6 s.

will be able to observe most ($\gtrsim 95$ per cent) of the accretion process on to a $10^5\,M_\odot$ MBH seed up to a comoving distance corresponding to $z \sim 25$, while *ATHENA* will only detect ~ 25 per cent of the total evolution, around the peak luminosity, up to $z \sim 15$.

Comparing the predicted peak flux (in the 1 keV observed band) with the CDF-S sensitivity, we find that this ultra-deep survey could have observed the accretion process on to a typical MBH up to $z_{max} \sim 15$. In the CDF-S survey, $N_C = 3$ active galactic nucleus (AGN) candidates at $z \gtrsim 6 \equiv z_{min}$ have been identified (Giallongo et al. 2015, but see also Weigel et al. 2015 where the authors question some of these candidates) inside a sky region of $\sim 170\,\text{arcmin}^2$. An upper limit for the number density of MBH seeds can be derived as

$$n_\bullet(6 < z < 15) \lesssim \frac{N_C}{\Omega_{CDF}\mathcal{V}\mathcal{D}\mathcal{F}}, \tag{5}$$

where $\Omega_{CDF} = 1.1 \times 10^{-6}$ is the sky fraction observed by the CDF-S, $\mathcal{V} = 2.3 \times 10^{12}\,\text{Mpc}^3$ is the comoving volume of the Universe between z_{min} and z_{max}, $\mathcal{D}$ is the duty cycle for accretion and $\mathcal{F} \equiv t_{det}/t_{obs}$ is the fraction of time during which the object is detectable within the time frame $t_{obs}(6 < z < 15) = 670\,\text{Myr}$, assuming a single episode of MBH growth at these redshifts.[4] The predicted flux, within the spectral range 0.5–2.0 keV, is above the CDF-S sensitivity between ~ 85 and $\sim 115\,\text{Myr}$, so that $t_{det} = 30\,\text{Myr}$ and $\mathcal{F} = 0.045$. Using these values we obtain the following upper limit for the number density of MBH seeds:

$$n_\bullet(6 < z < 15) \lesssim \frac{2.5 \times 10^{-5}}{\mathcal{D}}\left(\frac{0.045}{\mathcal{F}}\right)\,\text{Mpc}^{-3}. \tag{6}$$

Considering MBHs of initial mass $10^5\,M_\odot$ growing up to $\sim 10^7\,M_\odot$ (Pacucci & Ferrara 2015), we finally obtain the following upper limit for the MBH seeds mass density:

$$\rho_\bullet(6 < z < 15) \lesssim \frac{2.5 \times 10^2}{\mathcal{D}}\left(\frac{0.045}{\mathcal{F}}\right)\,M_\odot\,\text{Mpc}^{-3}. \tag{7}$$

The discussion so far has been limited to the scenario in which an MBH with an initial mass close to the peak of the birth mass function devised in Ferrara et al. (2014) accretes gas from an LDP host halo in the Eddington-limited mode. However, this is not the only possible scenario. Table 1 provides a general outline of the accretion history and CDF-S observability for an MBH seed with initial mass $10^5\,M_\odot$ in three additional scenarios: standard accretion – HDP, slim disc accretion – LDP and slim disc accretion – HDP. Table 1 includes the depletion time t_{end}, the duty cycle $\mathcal{D}$, the detection time t_{det} with its related value of $\mathcal{F}$ and the upper limit on $\rho_\bullet$. In the Eddington-limited cases the depletion times are lower limits since, while our simulations are run in isolation, in a cosmological framework the halo growth by mergers and accretion would not be negligible within $\sim 100\,\text{Myr}$. In the slim disc case, given the depletion times of order $\sim 10\,\text{Myr}$, the hierarchical growth of the halo plays a minor role.

Interestingly, the accretion process is undetectable by the CDF-S in the slim disk – LDP case, whose time-evolving spectrum is shown in Fig 4. Therefore no constraints on $\rho_\bullet$ can be obtained in this case.

The slim disk – HDP case is instead observable, albeit only for a very short time, $t_{det} \sim 1\,\text{Myr}$, due to the larger accretion rates in this scenario, which produce a sufficiently high luminosity despite

---

[4] This calculation assumes spherical symmetry of the host halo and an isotropic irradiation of the MBH. If the density along the poles is much lower, then a fraction of the sources would be completely unobscured.
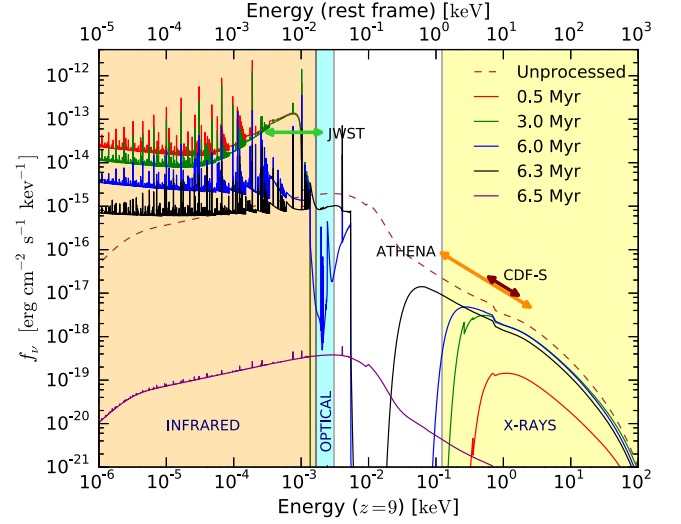

Figure 4. As in Fig. 3, but for the slim disk accretion – LDP case.

radiation trapping. The very low value of $\mathcal{F} \sim 1.5 \times 10^{-3}$ produces an upper limit for $\rho_\bullet$ higher than in other accretion scenarios by a factor ~ 35.

Let us now focus on the reason why the slim disc case leads to a very different value for $\rho_\bullet$ with respect to the standard accretion case. The amount of mass which is available for accretion is equal in both cases ($\sim 10^7\,M_\odot$) and, to a first-order approximation, also the mass actually accreted is similar. This is not strictly true, since the radiation pressure is more efficient in the standard case in creating mass outflows (Pacucci et al. 2015), but the produced outflows are fairly weak regardless of the accretion scenario. The real difference between the slim disk and the standard cases is due to radiation trapping, which decreases the effective bolometric luminosity (i.e. the luminosity escaping to infinity) in the former case, with respect to the latter. Since the accreting black hole is intrinsically fainter in the slim disk case, it will be observable for a smaller fraction of time, $\mathcal{F}$ (with the extreme $\mathcal{F} = 0$ for the LDP case), during its evolution: this eventually leads to a larger upper limit on $\rho_\bullet$.

The initial mass of the MBH seed influences the time-scale of the process and its observability. If, for instance, the high-redshift population of MBHs is characterized by a larger average mass, the evolutionary time-scale would be smaller (since $t_{end} \propto \dot{M}_{Edd}^{-1} \propto M_\bullet^{-1}$, where $\dot{M}_{Edd}$ is the Eddington accretion rate), but the emitted luminosity would be higher (since $L \propto L_{Edd} \propto M_\bullet$). The effect on $\mathcal{F}$ may vary from case to case, but in general a larger average mass is likely to decrease $\mathcal{F} \equiv t_{det}/t_{obs}$ since $t_{det} \leq t_{end} \propto M_\bullet^{-1}$. This would lead to a less stringent upper limit on $\rho_\bullet$.

4 DISCUSSION AND CONCLUSIONS

Using a combination of radiation-hydrodynamic and spectral synthesis codes, we have investigated the time-evolving spectral energy distribution of an accreting $z \sim 10$ MBH. The MBH seed, whose initial mass is $10^5\,M_\odot$, is embedded in a dark matter halo of total mass $10^8\,M_\odot$. Employing two gas density profiles and two accretion modes (Eddington-limited and slim disc) we simulated the system until complete gas depletion and we accurately calculated the time-evolving spectrum of the radiation emerging from the host halo. The main results of this work are summarized in the following.

(i) The spectrum of the emerging radiation, for an MBH observed at $z = 9$, is dominated by the infrared-submm (1-1000 μm) and

X-ray (0.1–100 keV) bands. Photons with frequency shortwards than the Lyα line are absorbed by the intervening matter at column densities $N_H \gtrsim 10^{23}$ cm^{-2} and reprocessed at lower energies, in the infrared band. Due to the very large mean free path $\lambda_X > 1$ Gpc of X-ray photons, growing MBH seeds negligibly contribute to reionization. The continuum normalization is set by: (i) the bolometric luminosity of the source and (ii) the column density of the host halo. The former determines the overall normalization, while the latter determines the ratio between the low-energy and the high-energy continua.

(ii) Our predictions show that the *JWST* will detect in the infrared a fraction $\gtrsim 95$ per cent of the accretion process on to a typical MBH seed observed at $z \sim 9$, while *ATHENA* should observe it in the high-energy bands only around the peak luminosity, a fraction ~ 25 per cent of the total evolution. Similarly, long-exposure surveys in the X-ray, like the CDF-S, could have already observed the accretion process on a $z \sim 9$ object for a comparable fraction of time. The redshift of the sources sets their luminosity distance, hence influences their detectability. For instance, the standard accretion – LDP system is observable by the CDF-S for ~ 41 per cent of the time at $z_{min} = 6$, while it becomes undetectable at $z \gtrsim z_{max} = 15$.

(iii) From the $z \gtrsim 6$ candidates detected in the CDF-S survey (Giallongo et al. 2015) we estimate the following upper limits on the $z \gtrsim 6$ MBH mass density: (a) $\rho_\bullet \lesssim 2.5 \times 10^2$ M$_\odot$ Mpc^{-3} assuming Eddington-limited accretion; (b) $\rho_\bullet \lesssim 7.6 \times 10^3$ M$_\odot$ Mpc^{-3} if accretion occurs in the slim disc, highly obscured mode. However, the accretion process is undetectable with the CDF-S sensitivity in the slim disc accretion – LDP case, due to the flux suppression caused by radiation trapping, and no constraints on $\rho_\bullet$ can be given.

Very recently, we proposed that the first detection of a high-redshift MBH seed could have already occurred. Indeed, in Pallottini et al. (2015) we showed that the observational features of CR7 (Sobral et al. 2015), a bright Lyα emitter at $z = 6.604$, may be explained by accretion on to an MBH of initial mass $\sim 10^5$ M$_\odot$.

For Eddington-limited accretion, our upper limit, $\rho_\bullet \lesssim 2.5 \times 10^2$ M$_\odot$ Mpc^{-3}, is compatible with the one set by Cowie et al. (2012) using observations of faint X-ray sources in the CDF-S, while it is more stringent than limits by Willott (2011), Fiore et al. (2012) and Treister et al. (2013) ($\rho_\bullet \lesssim 10^3$ M$_\odot$ Mpc^{-3}) and particularly by Salvaterra et al. (2012) ($\rho_\bullet \lesssim 10^4$ M$_\odot$ Mpc^{-3}, using the unresolved X-ray emission). The current observational constraints, however, do not take into account heavily buried, Compton-thick objects or radiatively inefficient accretion. Recently, indeed, Comastri et al. (2015) suggested that recent revisions to the local supermassive black holes' (SMBHs) mass density, up to $\rho_\bullet(z=0) \sim 10^6$ M$_\odot$ Mpc^{-3}, seem to imply that a significant fraction of the local SMBHs have grown in heavily buried, Compton-thick phases, or by radiatively inefficient accretion. Our model is a first step towards testing the role of Compton-thick or radiatively inefficient phases in the early growth of MBHs.

In the present paper, we provided a general picture of the interconnection between the main accretion mode at work in the high-redshift Universe and the black hole mass density. To summarize our rationale: assuming that, for MBHs at $z \gtrsim 6$, the main accretion channel is the standard, Eddington-limited one, we are able to provide an upper limit on $\rho_\bullet$ which is consistent (and competitive) with current estimates. In the standard disc scenario, MBHs have grown in heavily buried, Compton-thick phases for about 70 per cent of the total evolution time (e.g. ~ 70 Myr for the LDP), but they are long-lived and intrinsically bright, and visible for a substantial amount of time. Assuming instead that at supercritical accretion rates the

accretion disc thickens, with radiation trapping playing a significant role, the suppressed radiative efficiency leads to a much lower intrinsic luminosity. These sources are intrinsically faint, not obscured: the Compton-thick phase is short (~ 2 Myr, 30 per cent of the total evolution time for the LDP) because the obscuring gas is consumed rapidly. Our slim disk simulations suggest, as one would expect, that these short-lived and fainter MBHs are more difficult to detect in current surveys compared to brighter objects accreting in the Eddington-limited mode. As a consequence, the upper limit on $\rho_\bullet$ is inevitably higher than currently predicted, up to a factor ~ 35.

REFERENCES

Abramowicz M. A., Fragile P. C., 2013, Living Rev. Relativ., 16, 1
Abramowicz M. A., Czerny B., Lasota J. P., Szuszkiewicz E., 1988, ApJ, 332, 646
Agarwal B., Dalla Vecchia C., Johnson J. L., Khochfar S., Paardekooper J.-P., 2014, MNRAS, 443, 648
Begelman M. C., 1978, MNRAS, 184, 53
Begelman M. C., 2012, MNRAS, 420, 2912
Begelman M. C., Volonteri M., Rees M. J., 2006, MNRAS, 370, 289
Begelman M. C., Rossi E. M., Armitage P. J., 2008, MNRAS, 387, 1649
Blandford R. D., Begelman M. C., 1999, MNRAS, 303, L1
Bromm V., Loeb A., 2003, ApJ, 596, 34
Bromm V., Yoshida N., 2011, ARA&A, 49, 373
Choi J.-H., Shlosman I., Begelman M. C., 2015, MNRAS, 450, 4411
Comastri A., Gilli R., Marconi A., Risaliti G., Salvati M., 2015, A&A, 574, L10
Coughlin E. R., Begelman M. C., 2014, ApJ, 781, 82
Cowie L. L., Barger A. J., Hasinger G., 2012, ApJ, 748, 50
Ferland G. J. et al., 2013, Rev. Mex. Astron. Astrofis., 49, 137
Ferrara A., Salvadori S., Yue B., Schleicher D., 2014, MNRAS, 443, 2410
Fiore F. et al., 2012, A&A, 537, A16
Giallongo E. et al., 2015, A&A, 578, 83
Haiman Z., 2013, in Wiklind T., Mobasher B., Bromm V., eds, Astrophysics and Space Science Library, Vol. 396, Astrophysics and Space Science Library. Springer-Verlag, Berlin, p. 293
Jiang Y.-F., Stone J. M., Davis S. W., 2014, ApJ, 796, 106
Johnson J. L., Whalen D. J., Fryer C. L., Li H., 2012, ApJ, 750, 66
Lasota J.-P., 2015, preprint (arXiv:e-print)
Latif M. A., Schleicher D. R. G., Schmidt W., Niemeyer J., 2013a, MNRAS, 433, 1607
Latif M. A., Schleicher D. R. G., Schmidt W., Niemeyer J. C., 2013b, MNRAS, 436, 2989
Latif M. A., Niemeyer J. C., Schleicher D. R. G., 2014, MNRAS, 440, 2969
Lodato G., Natarajan P., 2006, MNRAS, 371, 1813
McKinney J. C., Tchekhovskoy A., Sadowski A., Narayan R., 2014, MNRAS, 441, 3177
McKinney J. C., Dai L., Avara M. J., 2015, MNRAS, 454, 6
Mineshige S., Kawaguchi T., Takeuchi M., Hayashida K., 2000, PASJ, 52, 499
Mortlock D. J. et al., 2011, Nature, 474, 616
Ohsuga K., Mineshige S., Mori M., Umemura M., 2002, ApJ, 574, 315
Pacucci F., Ferrara A., 2015, MNRAS, 448, 104
Pacucci F., Ferrara A., Marassi S., 2015, MNRAS, 449, 1076
Pacucci F., Volonteri M., Ferrara A., 2015, MNRAS, 452, 1922
Paczynski B., Abramowicz M. A., 1982, ApJ, 253, 897
Pallottini A. et al., 2015, MNRAS, 453, 2465
Planck Collaboration XIII et al., 2015, preprint (arXiv:e-print)
Sadowski A., 2009, ApJS, 183, 171

Sadowski A., 2011, preprint (arXiv:e-print)
Salvaterra R., Haardt F., Volonteri M., Moretti A., 2012, A&A, 545, L6
Sesana A., Volonteri M., Haardt F., 2007, MNRAS, 377, 1711
Sesana A., Gair J., Berti E., Volonteri M., 2011, Phys. Rev. D, 83, 044036
Shakura N. I., Sunyaev R. A., 1973, A&A, 24, 337
Shang C., Bryan G. L., Haiman Z., 2010, MNRAS, 402, 1249
Sobral D., Matthee J., Darvish B., Schaerer D., Mobasher B., Röttgering H., Santos S., Hemmati S., 2015, ApJ, 808, 139
Spaans M., Silk J., 2006, ApJ, 652, 902
Thorne K. S., 1974, ApJ, 191, 507
Treister E., Schawinski K., Volonteri M., Natarajan P., 2013, ApJ, 778, 130
Volonteri M., 2010, A&AR, 18, 279
Volonteri M., Bellovary J., 2012, Rep. Prog. Phys., 75, 124901
Volonteri M., Rees M. J., 2005, ApJ, 633, 624
Volonteri M., Lodato G., Natarajan P., 2008, MNRAS, 383, 1079
Volonteri M., Silk J., Dubus G., 2015, ApJ, 804, 148
Weigel A. K., Schawinski K., Treister E., Urry C. M., Koss M., Trakhtenbrot B., 2015, MNRAS, 448, 3167
Willott C. J., 2011, ApJ, 742, L8

Wu X.-B. et al., 2015, Nature, 518, 512
Yu Q., Tremaine S., 2002, MNRAS, 335, 965
Yue B., Ferrara A., Salvaterra R., Xu Y., Chen X., 2013, MNRAS, 433, 1556
Yue B., Ferrara A., Salvaterra R., Xu Y., Chen X., 2014, MNRAS, 440, 1263

SUPPORTING INFORMATION

Additional Supporting Information may be found in the online version of this article:

(http://www.mnras.oxfordjournals.org/lookup/suppl/doi:10.1093/mnras/stv2196/-/DC1).

Please note: Oxford University Press is not responsible for the content or functionality of any supporting materials supplied by the authors. Any queries (other than missing material) should be directed to the corresponding author for the article.

This paper has been typeset from a TeX/LaTeX file prepared by the author.